AN O_2^+ PRIMARY ELECTRON COLLISION ION SOURCE FOR THE STUDY OF HARPOONING TRANSITIONS AT SURFACES

PAN HAOCHANG (*), T. C. M. HORN, P. H. F. REIJNEN and A. W. KLEYN

FOM - Institute for Atomic and Molecular Physics,
Kruislaan 407, 1098 SJ Amsterdam, The Netherlands

(Received 3 October 1986; final form in 26 May 1987)

ABSTRACT — This paper describes a primary electron collision ion (Nier) source for producing an O_2^+ molecular beam, which is used in experiments to study harpooning transitions in the interaction of O_2^+ with a Ag (111) surface. The beam energy is 100-400 eV with an energy spread of about 0.01-0.03. The beam current density is about $10^{-10} - 10^{-9}$ A/cm^2 at a distance of 100 cm from the source. The O^+ fraction can be as mall as 0.01. The operation of the source in a surface scattering experiment is described. Some experimental results of harpooning transitions at surfaces are presented.

1 – INTRODUCTION

Harpooning reactions are well known chemical reactions in the gas phase [1]. The reactions proceed via an ionic intermediate, e. g. $K + Br_2 \rightarrow K^+ + Br_2^- \rightarrow KBr + Br$. The ionic intermediate can be formed at the crossing seam of the potential energy surfaces for the neutral (covalent) and ionic states at large separation of the reactants. The formation of free ion-pairs has been observed as soon as there is enough energy to form the pair in an (endothermic) harpooning reaction. From studies of ion-pair formation much information has been obtained about the understanding of harpooning reactions [2]. Research of this type is also currently being performed in Portugal by Moutinho's group [3].

(*) Permanent address: Institute of Nuclear Research, Academia Sinica, P. O. Box 8204, Shanghai, China.

For collisions in the gas phase the electron jump can enlarge the reactive cross section considerably with respect to gas-kinetic cross sections. In molecule-surface collisions this increase is irrelevant, because the molecule will hit the surface anyway. In surface collisions the importance of harpooning is that it turns on an attractive force, i. e., the electrostatic image force, that can initiate trapping, sticking, dissociation or even a reaction of the molecule, whereas otherwise elastic scattering occurs. This is indicated schematically in Fig. 1. Theoretical work has indicated

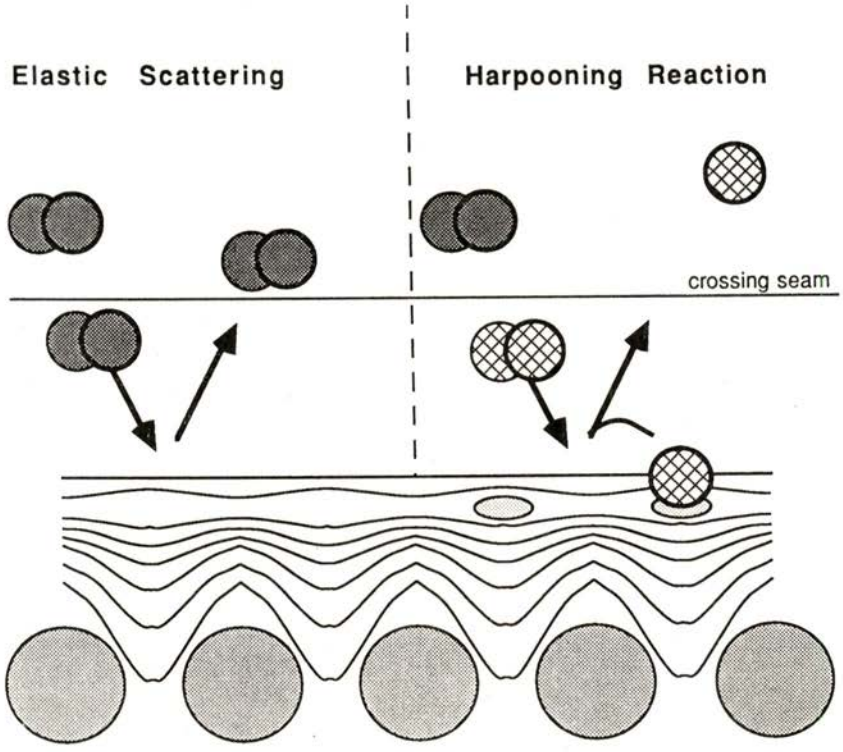

Fig. 1 — Schematic representation of a harpooning-reaction at a surface. A sideview of a part of the surface with 5 atoms is given. The contours around the atoms indicate the potential energy for the incoming particle. At the left an elastic collision is shown. At the right the molecule picks up an extra electron after passing the crossing seam. An attractive force is turned on, which is strongest in the egg-shaped regions. The situation drawn represents the case when the molecular bond is weakened by the harpooning, which results in dissociation of the molecule and subsequent sticking of an atom. The picture does not refer to any particular situation encountered experimentally.

that harpooning can occur in molecule surface collisions [4]. The curve crossing needed could be induced by the electrostatic image force.

To study the dynamics of harpooning at surfaces one should perform experiments in which the important step of the reaction, i. e. the negative ion formation, occurs and in which the collision energy is sufficiently high to prevent subsequent sticking. O_2 scattering from Ag is a good system for the study of these processes. It is known that molecularly chemisorbed O_2 is negatively charged [5]. Consequently, the neutral state of the system can be expected to cross the potential of the ionic ($Ag^+ + O_2^-$) at a reasonably large molecule-surface distance. Therefore we have studied O_2 scattering from Ag [6]. Because it is very difficult to make O_2 beams in the eV range. we use an O_2^+ beam, assuming that it neutralizes into the ground state of O_2 when approaching the surface. Energetic beams are necessary because the process of negative ion formation is endothermic by a few eV.

The experimental setup is a modified version of the one used by Tenner et al. [7] to study alkali ion scattering. The positive ions are produced by an electron impact ionization (Nier) type gun that will be described in detail in this paper. The crystal is mounted in a two axis goniometer. The scattered ions are detected using a 90° cylindrical electrostatic energy analyzer, which can be rotated around the crystal. The set-up is shown schematically in Fig. 2.

The requirements for the ion source are as follows:

(1) The beam should consist exclusively of O_2^+.

(2) Because it is connected, via a pumping resistance, with an UHV chamber, with a base pressure of 1×10^{-10} mbar, the working pressure of the source chamber should be around 10^{-6} mbar.

(3) The source should operate at a distance from the target of about 100 cm.

(4) A small energy spread of the ion beam is required for studying dynamics of surface processes.

(5) Finally, although the gas introduced into the source is oxygen, the filament should have a reasonable lifetime.

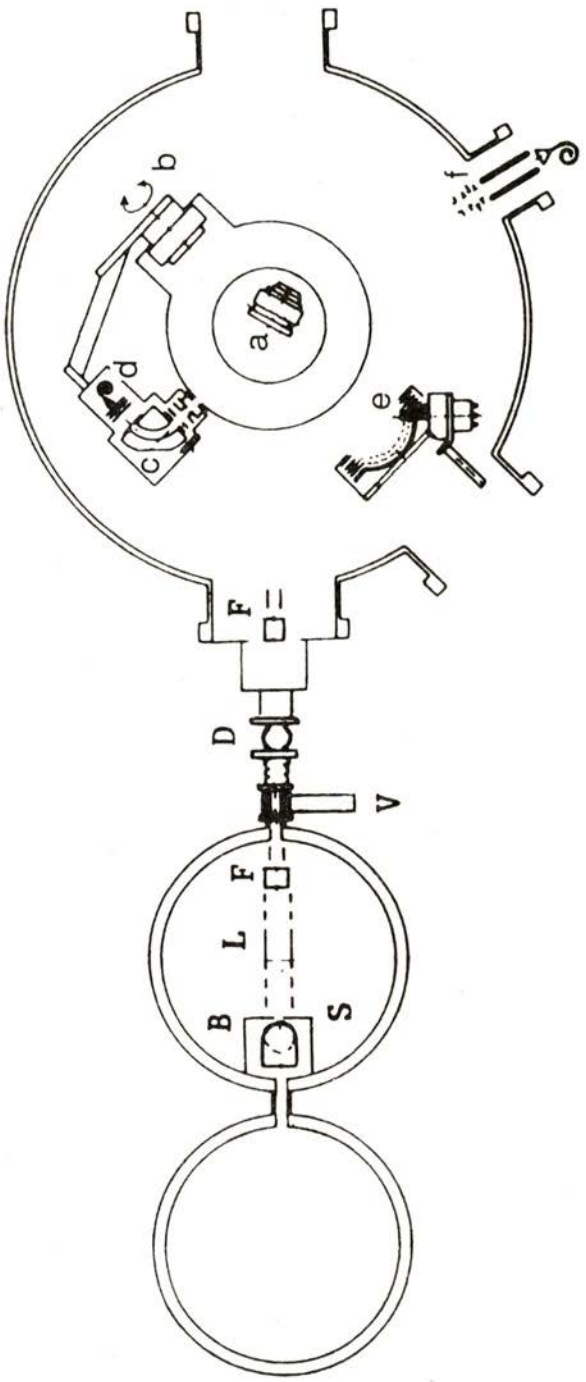

Fig. 2 — A schematic diagram of the experimental set-up. The source part contains the following elements: S = ion source, B = screen box, L = lens system, F = deflectors, V = valve and D = diaphragm. The UHV chamber contains: a = target manipulador, b = detector manipulator, c = energy analyzer, d = open channeltron, e = LEED system and f = quadrupole residual gas spectrometer.

Based on the requirements mentioned above we have decided to use a primary electron collision ion (or Nier) source [8]. A useful overview of available ion sources is given in [9].

In the following sections we will describe: the principle and construction of the ion source in section 2, measurement of the beam current and factors which influence the beam current in section 3, measurement of energy spread of the ion beam in section 4, measurement of ratio $O^+ / (O_2^+ + O^+)$ by using a Wien filter in section 5, the application of the source in surface scattering experiments in section 6, some results on harpooning transitions in section 7, and conclusions in section 8.

2 — PRINCIPLE AND CONSTRUCTION

In a primary electron collision ion source atomic or molecular ions are created by collisions of energetic electrons with gas molecules. There are four steps in the process: (1) Production of electrons by thermal emission and acceleration of the electrons to a certain energy; (2) Production of ions by collisions of the energetic electrons with gas molecules in a small ionization chamber; (3) Extraction of the ions from the ionization chamber and their acceleration to the required energy; (4) Focusing and transmission of the ion beam by a lens system. The pressure in the chamber being low enough and the electron beam sufficiently confined (by an axial magnetic field) no double collisions of electrons or ions occur. This is in contrast to plasma sources.

When electrons collide with gas molecules several processes may happen according to the electron energy, such as elastic collisions, excitation or ionization of gas particles, or dissociation of gas molecules. If the energy of the primary electrons greatly exceeds the ionization energy of the particles, multiple ionization may occur.

In order to produce an O_2^+ ion beam the electron energy should be higher than the ionization energy of O_2^+ (12 eV) and should not be too high to avoid dissociation of molecules, production of O^+ and multiple ionization [10].

When an electron beam passes through a gas the ion yield is given by [11]:

$$n_+ = j^- \; p \, l \, S_e / e \qquad (\mathrm{cm^{-2}\,s^{-1}}) \tag{1}$$

where j^- is the electron current density (A/cm^2), p is the gas pressure (Torr), l is the length of the electron beam in the ionization volume (cm), and S_e is the differential ionization coefficient (cm^{-1} $Torr^{-1}$), which depends on electron energy and gas species.

Fig. 3 illustrates our O_2^+ ion source. The filament F is a pure rhenium ribbon with dimension $6 \times 0.07 \times 0.05\ mm^3$. The operating current is 6A. The electron energy is determined by V_e, the voltage between the filament and the ionization chamber. The emission of the filament consist of the electron beam entering the ionization chamber and the electrons hitting the outside wall of the chamber. To obtain an emission limited beam the distance between the filament and the ionization chamber is smaller than 1 mm. The ionization chamber is a small stainless steel box, of depth and diameter 8 mm and 15 mm, respectively. It has an electron entrance, a gas inlet, a repeller, a hole facing a collector and an exit through which the ions are extracted from the ionization chamber. The ion beam energy is determined by V_{ext}, the voltage between the extractor and the ionization chamber. The distance between the extractor and the ionization chamber is about 7 mm. In front of the exit, at a distance of 1 mm, there is a slit which consists of two plates which can be supplied with different voltages to deflect and focus the beam. In addition, those voltages can make the extraction field more homogeneous. If the repeller inside the ionization chamber is put at a positive potential, V_{rep}, with respect to the chamber, the repeller can increase the extraction efficiency of ions, enhancing the beam current effectively, but this will influence the energy spread of the ion beam.

A strong magnetic field parallel to the electron beam makes the electrons spiral and will increase the electron path length in the ionization chamber (see Fig. 3; M is a permanent magnet). The magnetic field strength is 500 G near the magnet and 150 G at the center of the ionization chamber.

The distance from the source to the target in the UHV chamber is about 100 cm. A lens system L is used to improve the

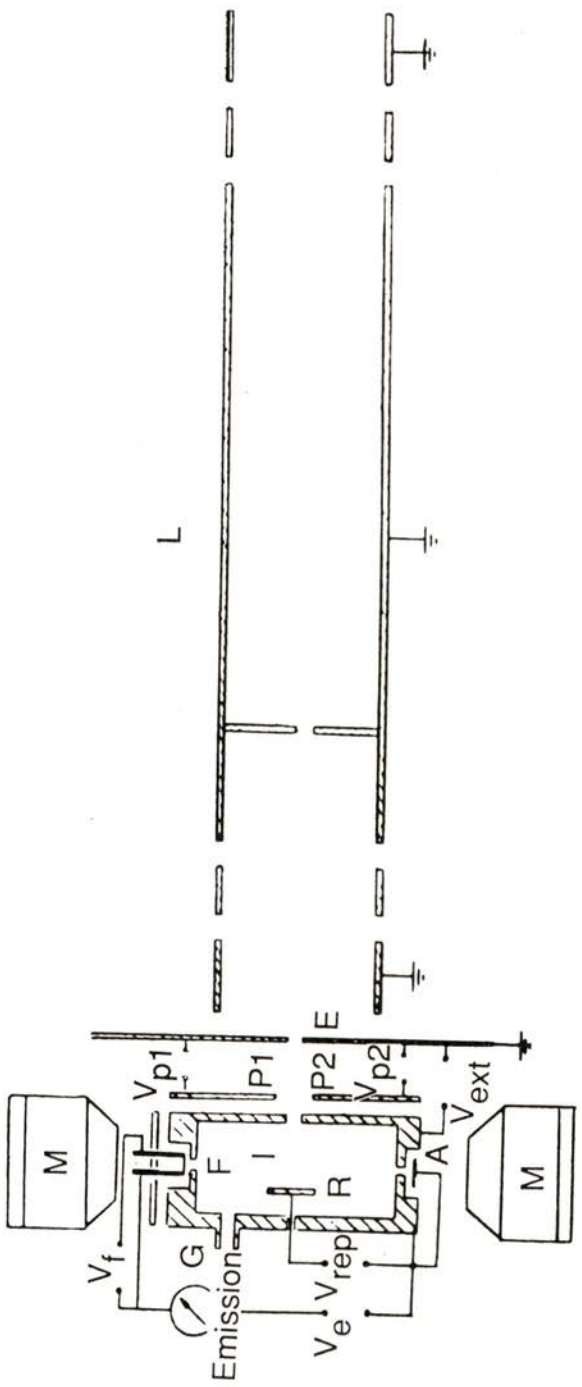

Fig. 3 — A schematic diagram of the ion source and the lens system: I = ionization chamber, F = filament or cathode, G = gas inlet, E = extractor, P1 and P2 = focusing plates, R = repeller, A = collector, M = magnet and L = lens system.

beam current density. The lens system has two lenses which are made up of five cylinders of 20 mm diameter. The first, third and fifth cylinder are grounded. At the end of the lens system and at the entrance of the UHV chamber X and Y deflectors are mounted. Between the source chamber and the UHV chamber there is a pumping resistance, a pipe 5 mm in diameter and 40 mm long.

To test the performance of the source, measurements of the beam intensity, its energy spread and its composition have been performed. For measuring the beam intensity a wire or a plate collector is mounted in the wall of the source chamber after the lens system and the X and Y deflectors. A grid is mounted between the deflector and collector to measure the energy distribution of the beam using the retarding method. The set-up to measure the energy spectra and composition of the beam is shown in Figure 4.

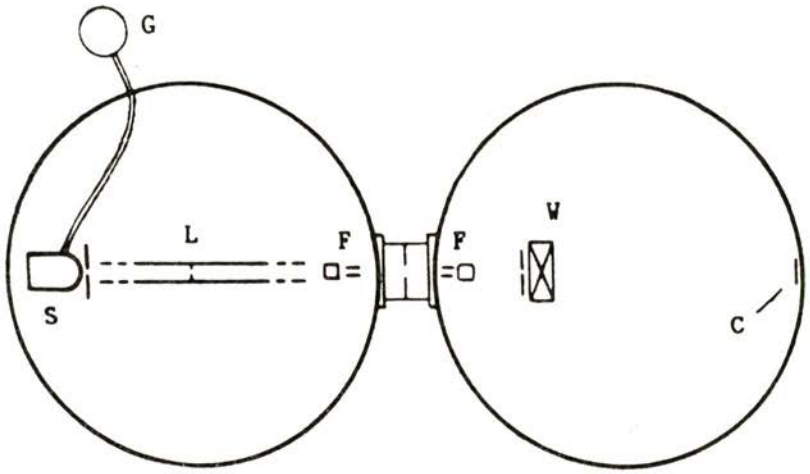

Fig. 4 — A schematic diagram of the test set-up to measure the energy spread and the composition of the beam, where S = ion source, G = gas bottle, L = lens system, F = deflectors, W = Wien filter and C = wire collector.

At the entrance of the second vacuum chamber there is another pair of X and Y deflectors. A wire collector is mounted at the other side of this chamber. A Wien filter behind a 1 mm diaphagm is placed near the deflectors.

3 – MEASUREMENT OF THE ION BEAM CURRENT

There are several factors which can influence the ion beam current (I), such as the emission of the filament, the electron energy, the extractor voltage, the repeller voltage and the voltages on the lens system. In order to make the best choice for those parameters, the dependence of I on the above-mentioned factors has been measured.

Fig. 5 shows the dependence of I on the emission. According to equation (1) I is proportional to emission. The small deviation of the curve from a straight line may be due to effects of the

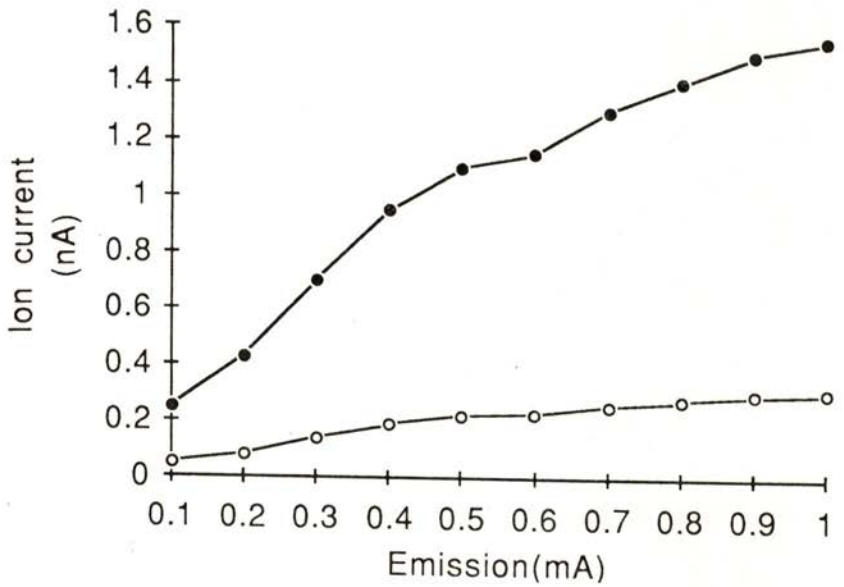

Fig. 5 — The ion current as a function of the emission; $p(O_2) = 5.10^{-6}$ torr, $V_e = 60$ V, $V_{ext} = 100$ V, $V_{rep} = 0$ V (open dots) or 20 V (filled dots).

change of the shape of the electron beam with emission, but the source can be operated at all emission values. So the choice of the operating value of the emission is limited by the lifetime of the filament. The suggested emission value is 0.5 to 2.0 mA. The current measured on the collector is about 0.1 of the emission current, which may be due to the fact that most electrons are not entering the ionization chamber at all.

Fig. 6 shows the dependence of I on the repeller voltage (V_{rep}). The decrease of I at the beginning of the curve can be explained as follows. When a positive voltage is added on the

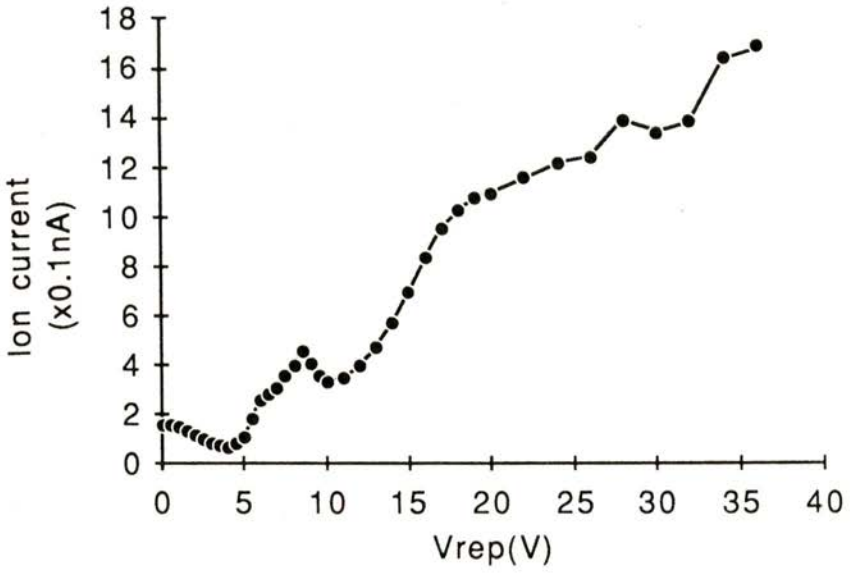

Fig. 6 — The ion current as a function of the repeller voltage; p (O_2) = 3.10^{-6} torr, Emission = 0.5 mA, V_e = 60 V, V_{ext} = 100 V.

repeller, it attracts electrons, which decreases the electrons beam intensity. At low V_{rep} the effect of attracting electrons is larger than the effect of repelling ions. When choosing V_{rep} its influence on the energy spread of the ion beam should be taken into acount. This will be discussed in section 4.

Fig. 7 shows the dependence of I on the extraction voltage V_{ext} . Above a threshold, I increases proportionally to V_{ext} . When the extractor voltage is lower than the threshold, I will almost be zero. So it is not possible to get an ion beam with energy lower than 20 eV. Of course, the choice of V_{ext} is determined by the required ion beam energy. By using a Heddle lens system [12] it is possible to increase the energy range of operation considerably.

Fig. 8 shows the dependence of I on V_e . Its shape is similar to the results published earlier [11].

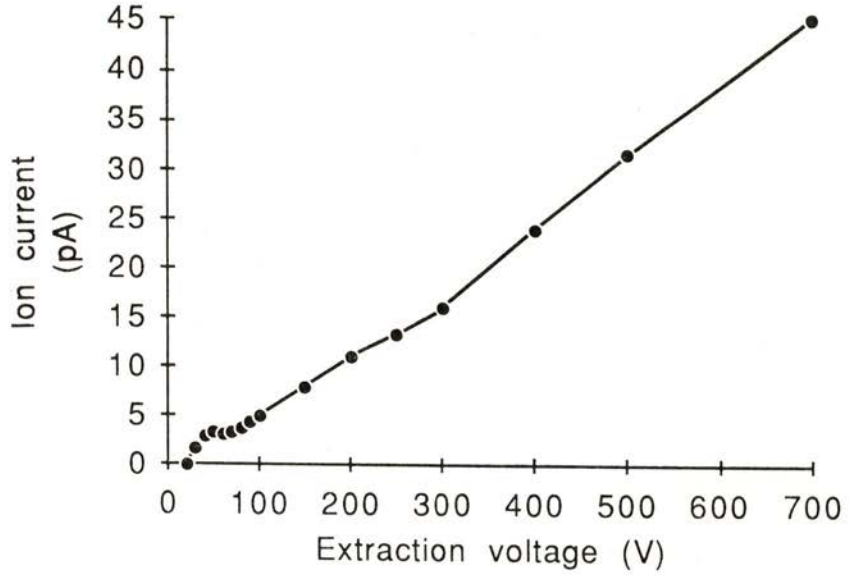

Fig. 7 — The ion current as a function of the extraction voltage; p (O_2) = 3.10^{-6} torr, Emission = 0.2 mA, V_{rep} = 0 V, no voltages applied on the lens system.

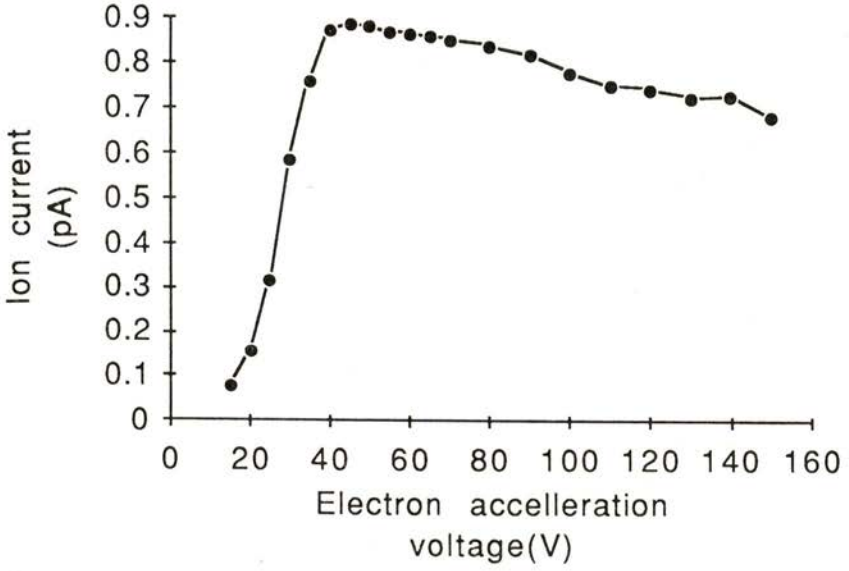

Fig. 8 — The ion current as a function of the electron acceleration voltage; p (O_2) = 3.10^{-6} torr, Emission ≃ 0.2 mA (the emission was adjusted for each point), V_{ext} = 100 V, V_{rep} = 0.07 V.

4 — MEASUREMENT OF THE ENERGY SPREAD OF THE ION BEAM

In experiments to study the dynamics of surface scattering a small energy spread of the ion beam is required. We used a retarding method to measure the energy spread. A grid is mounted at the end of the lens system. Behind the grid is a collector which is a wire of 0.5 mm diameter or a plate. The measured (integral) curves and the differentiated curves (directly showing the energy distribution) are presented in Fig. 9. The measurements are performed with focussing plate voltages $V_{p1} = V_{p2} = 0$. With a plate collector the energy spread is about 0.015 when $V_{rep} = 0$ V and about 0.029 when $V_{rep} = 15$ V. Another characteristic of these curves is that they all have a small peak at an energy lower than the main peak. The origin of this peak is not clear. Energy spectra of the beam have been measured using the energy analyser in the UHV chamber. Due to its worse resolution (0.1) the effects seen in Fig. 9 have not been confirmed (see also Fig. 13).

An appreciable repeller voltage can obviously increase the spread in beam energy. If $V_{rep} = 0$ V every point in the ionization chamber has equal potential. In addition, in the ionizing collisions the ions hardly can get any momentum from the electrons due to the large mass difference. Consequently, we can get a very small energy spread of the ion beam. But if V_{rep} is not zero, there will be a potential distribution between the repeller and the exit of the ionization chamber. Then, the ions extracted from different points inside the chamber will have different energy, which causes an increase of the energy spread.

5 — MEASUREMENT OF THE RATIO $O^+ / (O_2^+ + O^+)$ USING A WIEN FILTER

A Wien filter is a velocity selector for an ion beam [13]. It consists of an electric field E, and a magnetic field B, perpendicular to each other. An ion moving in a direction perpendicular to both fields experiences an electric and a magnetic force, which balance when the velocity is $v = E/B$; ions with this velocity pass through the Wien filter without deflection. Ions with a different velocity will be deflected. By fixing B and scanning E, a velocity spectrum can be obtained. The velocity resolution depends on the magnitude

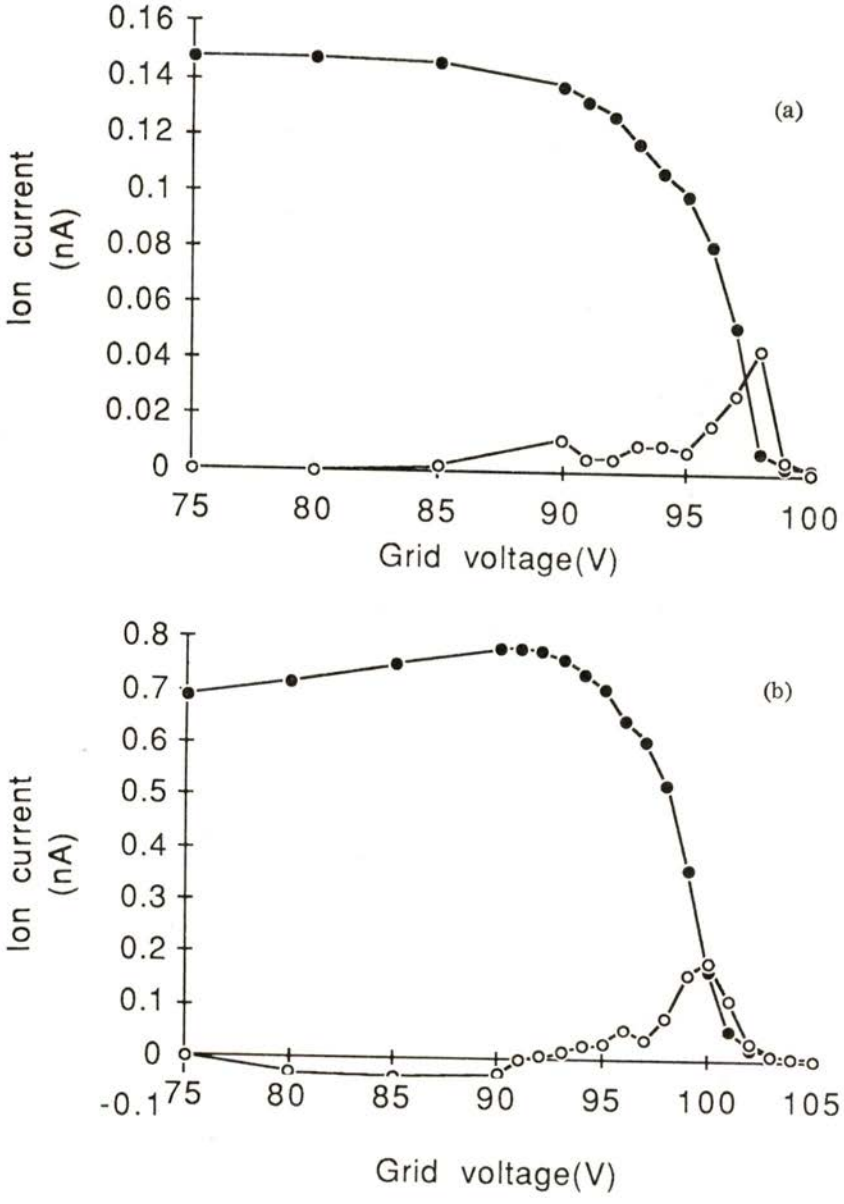

Fig. 9 — The ion current as a function of the retarding grid voltage (filled dots), measured using a plate collector and different repeller voltages; the differentiated curves (open dots) give the energy spread of the beam. $p(O_2) = 3.10^{-6}$ torr, Emission = 0.5 mA, $V_e = 60$ V, $V_{ext} = 100$ V, $V_{rep} = 0$ V (a) or $V_{rep} = 15$ V (b).

of E and B, the length of the Wien filter, the diameter of the diaphragm which is in front of the Wien filter, the size of the beam collector and the distance between the Wien filter and the beam collector.

Figure 10 shows the velocity spectra of O_2^+ and O^+ as a function of the voltage generating the electric field. Figures 11 and 12 show some velocity spectra of He^+, Ar^+ and Ar^{++}. The velocity spectra of He^+, Ar^+ and Ar^{++} are measured to calibrate the velocity or mass scale. Table 1 presents the mass assignment of the species associated with the peaks in figures 10-12, according to I_B, V_E, and beam energy, E_i. I_B is the current in the coil generating the magnetic field, V_E is the voltage associated with the electric field and v is the velocity of the ions, which is proportional to V_E / I_B, ($E_i = 200$ eV). The mass M is proportional to $E_i V^{-2}$ or $E_i (V_E / I_B)^{-2}$. Using the calibration by He^+ and Ar^+ we obtain the mass of the main peak in Fig. 10. It is about 32, which means that the beam consists of O_2^+.

The O^+ fraction is determined by V_e in the ionization process. Table 2 shows the ratio $O^+ / (O_2^+ + O^+)$ which is cal-

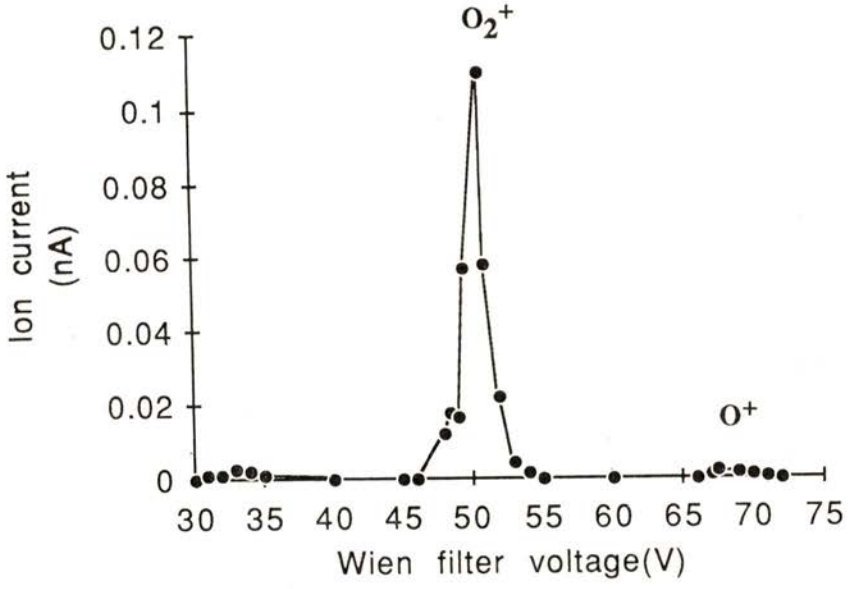

Fig. 10 — Velocity spectra of oxygen as a function of the Wien filter voltage, when a wire collector is used; $p(O_2) = 6.10^{-6}$ torr, $V_e = 50$ V, $V_{ext} = 200$ V, $V_{rep} = 0$ V, $I_B = 1.5$ A.

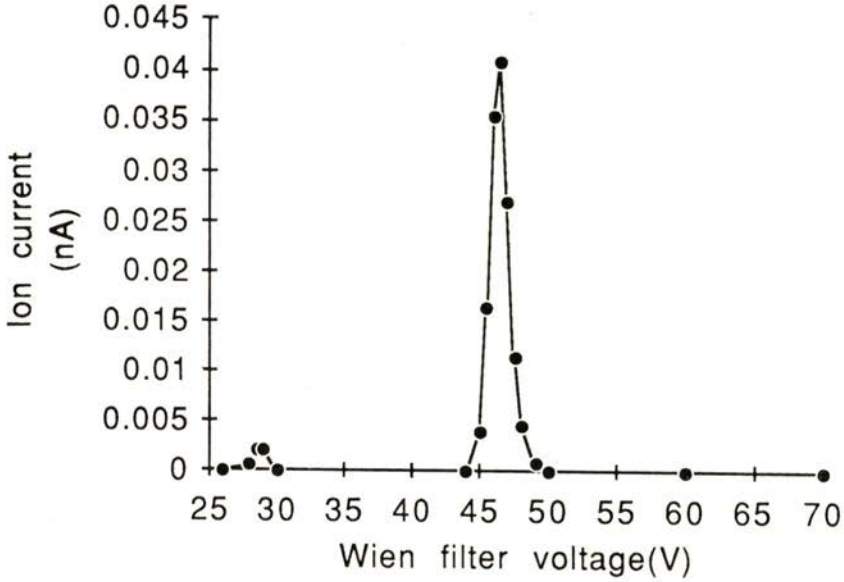

Fig. 11 — Velocity spectrum of helium as a function of the Wien filter voltage, when a wire collector is used; p (He) = 7.10^{-6} torr, $V_e = 60$ V, $V_{ext} = 200$ V, $V_{rep} = 0$ V, $I_B = 0.5$ A.

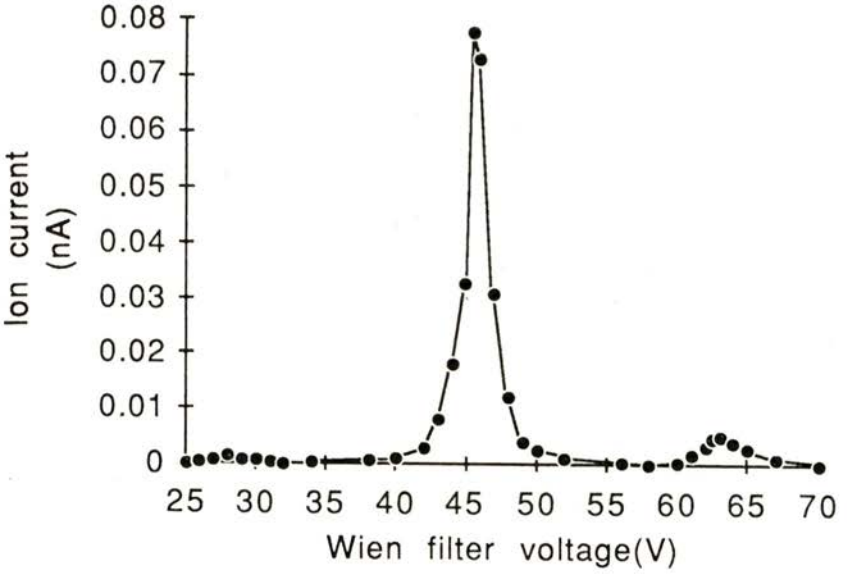

Fig. 12 — Velocity spectrum of argon as a function of the Wien filter voltage, when a wire collector is used; p (Ar) = 6.10^{-6} torr, $V_e = 60$ V, $V_{ext} = 200$ V, $V_{rep} = 0$ V, $I_B = 1.5$ A.

culated from the velocity spectra of O_2^+ and O^+ at several V_e values. Near each O_2^+ or O^+ peak there is a small shoulder at slightly lower velocity, visible in Fig. 10. This corresponds to the

TABLE 1 — The assignment of the mass M for the peaks in Figures 10-12

I_B (A)	V_E (V)	V_E / I_B ($\propto$ v)	Energy/v^2 ($\propto$ M)	Assignment of M
0.50	46.5	93.0	0.023	4 (H_e^+)
1.50	45.5	30.3	0.22	40 (Ar^+)
1.50	63.0	42.0	0.11	40 (Ar^{++})
1.50	50.2	33.5	0.18	32 (O_2^+)
1.50	69.0	46.0	0.09	16 (O^+)

TABLE 2 — The O^+ fraction in the oxygen beam for different values of the electron energy

V_e (V)	20	30	40	50	60	80
$O^+ / (O_2^+ + O^+)$ (%)	0	0.78	0.84	1.55	2.36	9.8

small peak in the energy spectra in Fig. 9. The origin of these small peaks is not known. The origin of the peaks at much lower E, around 30 V, may be due to hydrocarbon contaminants.

6 — APPLICATION OF THE SOURCE IN SURFACE SCATTERING EXPERIMENTS

After the experiments described, the source was aimed at a Ag (111) crystal in the UHV chamber of the MOBI apparatus, as shown in Fig. 1. Because of space limitations, the Wien filter, which was not really necessary for O_2^+ beams, has not been used.

Operating conditions of the source for 100, 200, 300 and 400 eV O_2^+ beams are listed in Table 3. The energy spectra of the beam, directly measured by the 90° cylindrical electrostatic energy analyser in the UHV chamber, are shown in Fig. 13. The width

Table 3 — Operating conditions for the O_2^+ beam used in the experiments

E_i (eV)	V_e (V)	V_{ext} (V)	V_2 (V)	V_4 (V)	V_{p1} (V)	V_{p2} (V)	emission (mA)	P_1 (10^{-6} torr)	P_2 (10^{-9} mbar)	I (10^{-9} A)
100	40	100	98	65	50	46	1.9	5	4	.15
200	40	200	196	122	79	72	2	5	4	.65
300	40	300	277	161	145	135	1	4.6	4	1
400	40	400	359	211	323	321	1	5	4	.8

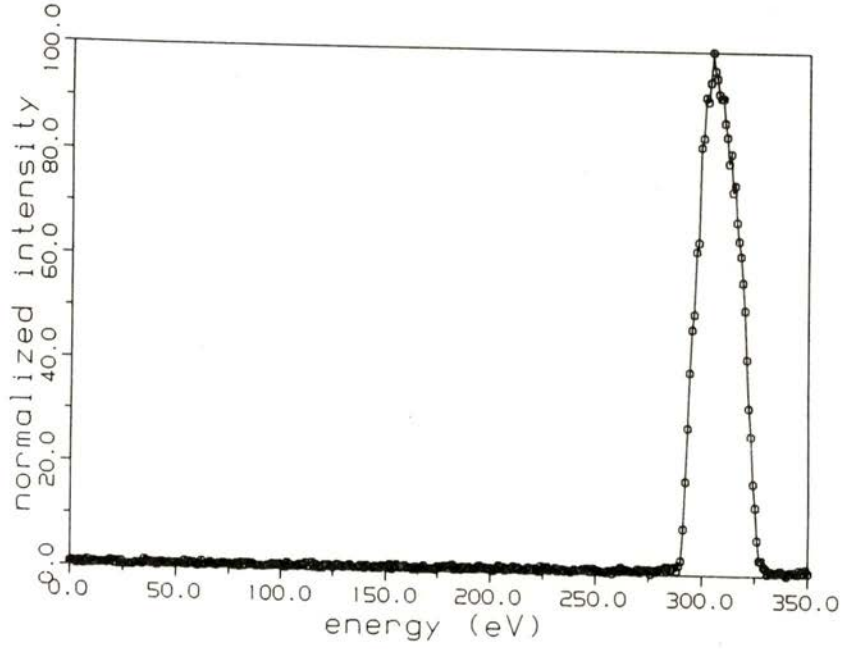

Fig. 13 — A measurement of the energy spectrum of the oxygen beam of 300 eV measured directly by the 90° cylindrical electrostatic energy analyser in the UHV chamber.

of the peak is determined by the resolution of the energy analyser ($\delta E/E \simeq 0.1$), and is much larger than seen in Fig. 9.

In $O_2^+ - Ag(111)$ surface scattering experiments, scattered ions could get negatively charged [6]. A typical energy spectrum of negative ions (O_2^- and O^-) after specular scattering of 300 eV O_2^+ from Ag (111) at an angle of incidence of 70 degrees with respect to the surface normal is shown in Fig. 14. The peak at

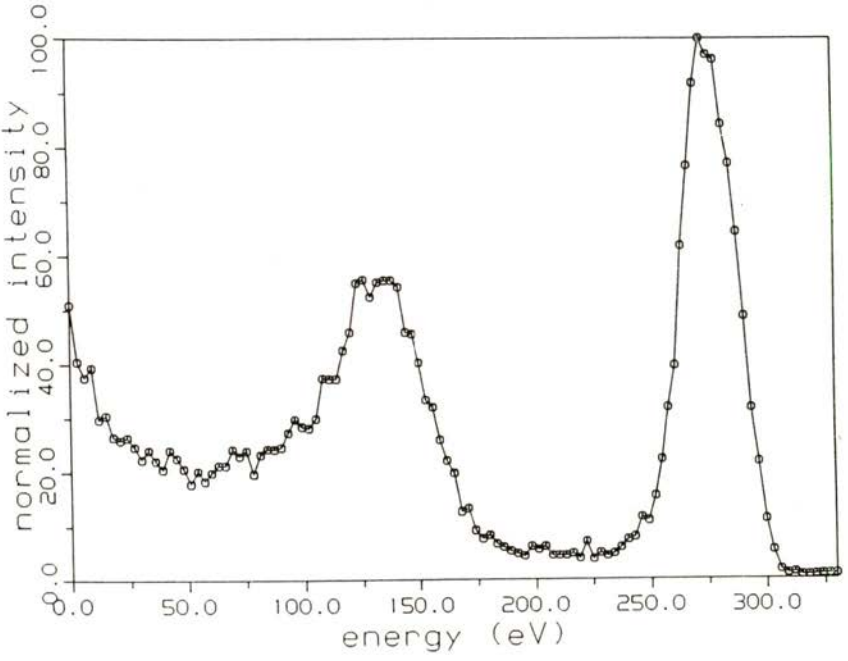

Fig. 14 — A typical energy spectrum of negative ions (O_2^- and O^-) after scattering of 300 eV O_2^+ from Ag (111), when the angles of incidence and detection (with respect to the surface normal) are both equal to 70 degrees.

275 eV is assumed to be O_2^- since it corresponds to an oxygen molecule having roughly lost the energy corresponding to two binary collisions with silver atoms as a consequence of the glancing incidence. The peak at half this energy is correspondingly due to O^-, carrying about half of the energy of the molecule [14].

Scanning the azimuth of the crystal over 360° shows a very nice symmetry corresponding to the hexagonal structure of the unit cell of Ag (111). This azimuthal dependence of O_2^- peak is shown in Fig. 15. The symmetry of this spectrum nicely shows that the crystal has been prepared properly, and turned out to be much more sensitive to the quality of the crystal surface than low energy electron diffraction (LEED).

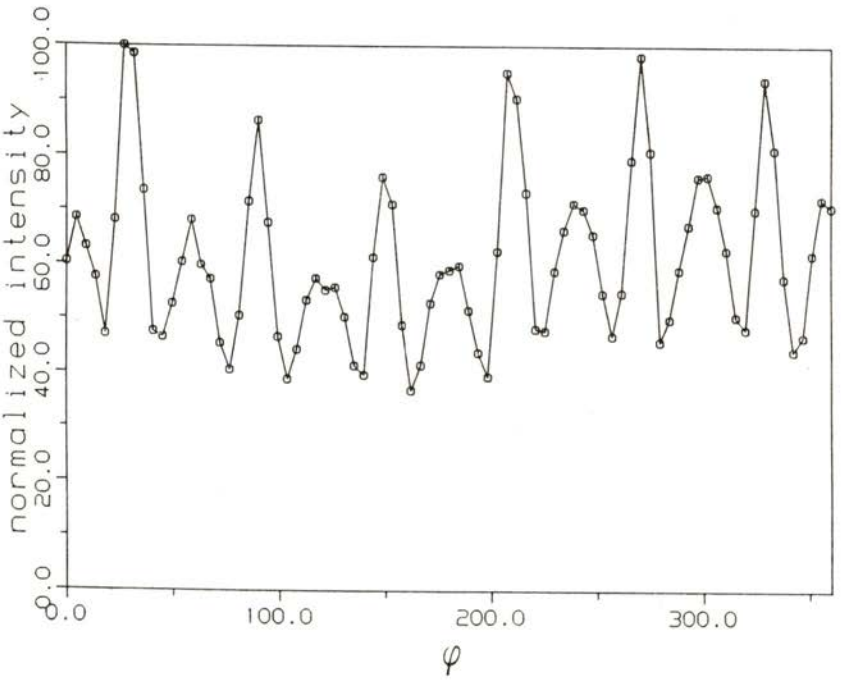

Fig. 15 — The azimuthal dependence of the O_2^- peak from the scattering as measured in fig. 14.

The O_2^+ beam seems pure because of the low background measured between the O_2^- and O^- peaks. O_2 gas efficiently removes contamination from the source, whereas in case of, for example, Ne the beam may contain H_2O^+, hydrocarbon ions and oxide ions. So, for those species a Wien filter is necessary.

7 — HARPOONING TRANSITIONS

The result for scattering of a beam of O_2^+ with an energy of 300 eV from Ag (111) leading to negative ions is shown in Fig. 16. The angle of incidence Θ_i measured from the surface normal is 70°. The figure shows the angular and energy spectrum of the negative ions. Two peaks are visible, at 130 and 275 eV,

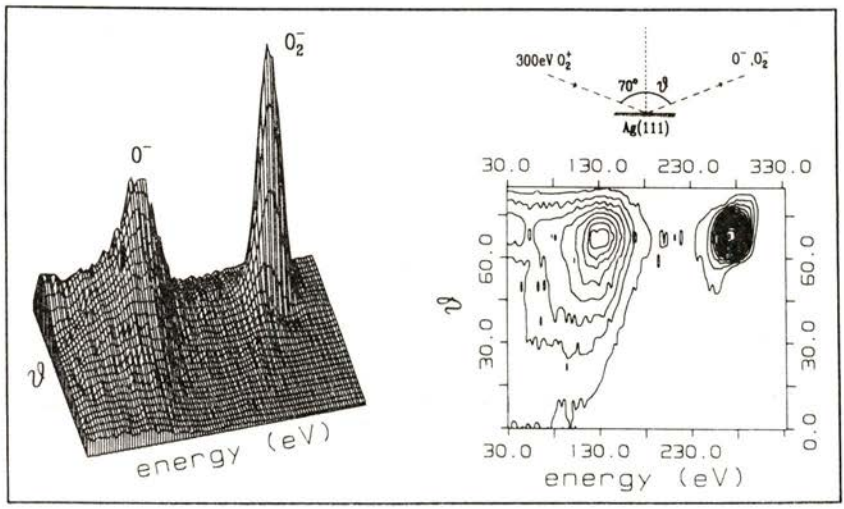

Fig. 16 — Intensity distribution for negative ions formed in glancing collisions ($\Theta_i = 70°$) of 300 eV O_2^+ ions with Ag (111). The measured intensity is plotted 3-dimensionally and in contour representation as a function of the final energy and polar scattering angle. The axes are identical for both representations. No correction for the energy dependent transmission of the energy analyser has been made. The inset shows the scattering geometry and the definition of the angles.

for the specular direction. These clearly can be identified with O^- and O_2^-, assuming that for scattered O^- each of the atoms carries half of the translational energy of the corresponding O_2^-. By varying the incident energy and Θ_i we find that the O^- yield seems to scale with the normal component of the impact velocity, and can exceed the O_2^- yield.

The count rates are an order of magnitude lower for positive than for negative ions. This large negative to positive ion ratio indicates that the probability for negative ion formation dominates and that negative ions are not formed at defect sites. A crude estimate shows that the total scattered negative ion yield is of the order of a few percent of the primary beam. The scattered neutrals could not be detected in our apparatus.

Three important events take place during the collision: 1) the neutralization of the positive ion, 2) the (hard) collision with the surface, 3) the attachment of a second electron. It seems likely that the first event occurs before the other two. For the first step resonant neutralization followed by Auger deexcitation and Auger neutralization are the most likely processes in view of the low beam energy. This would lead to neutralization into molecules in the ground state, which in turn leads to O_2^-. A subsequent event is the hard collision. The probability for impulsive energy transfer in this collision, leading to dissociation, seems small for specular scattering. However, classical trajectory calculations indicate that the dissociation of O_2^- observed in the figure can entirely be due to the collision with the surface. Calculations with an ab-initio potential show even more dissociation than observed experimentally [15]. This suggests that the most important step, i. e., the attachment of another electron to the molecular ion or atomic ions, proceeds more easily when molecular ions are the final product. It could be due to an orientational dependence of the charge transfer probabilities.

Having demonstrated that harpooning transitions occur for the O_2 / Ag (111) system, we now turn to the relevance of our observations to chemisorption. It is very likely that, for a slow O_2 molecule approaching the surface, the harpooning transition can take place along the way towards the surface, leading to chemisorption as O_2^-. A potential diagram suggested by Campbell indicates that the binding energy of O_2^- to Ag (111) is 0.3 eV [16]. The low sticking probability of O_2, in the order of 10^{-6}, indicates that the negative ion state is not accessible for thermal molecules, because of a barrier. Clearly the high translational and possibly also vibrational energy of the initial O_2^+ is sufficient to overcome this barrier, since the O_2^- relative yield is much larger than 10^{-6}. It also indicates that indeed the harpooning transition is responsible for the chemisorption of molecular oxygen on Ag surfaces. From

this we conclude that the importance of harpooning transitions in energy transfer processes at surfaces has been established experimentally and will add another dimension to these processes which traditionally are being thought of as collisions of hard spheres.

8 — CONCLUSION

The performance parameters of the O_2^+ ion source considered in this paper are the beam current and its current density, the energy and energy spread, the pressure in the source chamber and the lifetime of the filament. The source parameters we generally used are as follows: $V_e = 40\text{-}50$ V, resulting in $O^+ / (O_2^+ + O^+) \simeq 0.01$; the lifetime of the filament is a few tens of hours (it takes about 1 hour to change the filament); the beam current density is about $10^{-10} - 10^{-9}$ A/cm^2 at a distance of 100 cm.

Using this source, a significant contribution to the understanding of the dynamics of chemisorption of molecules at surfaces has been made, via the observation of so-called harpooning transitions.

Dr. H. Geerlings is thanked for his critical reading of the manuscript. This work is part of the research program of the Stichting voor Fundamenteel Onderzoek der Materie (Foundation for Fundamental Research on Matter) and was made possible by financial support from the Nederlandse Organisatie voor Zuiver Wetenschappelijk Onderzoek (Netherlands Organization for the Advancement of Pure Research). Partial support from the Koninklijke Shell Laboratorium Amsterdam is also gratefully acknowledged.

REFERENCES

[1] D. R. HERSCHBACH, *Adv. Chem. Phys.* **10** (1966), 319.
[2] A. W. KLEYN, J. LOS and E. A. GISLASON, *Phys. Repts.* **90** (1982), 1.
[3] A. M. C. MOUTINHO, *Portgal. Phys.* **15** (1984), 157;
E. E. B. COWAN, M. A. D. FLUENDY, A. M. C. MOUTINHO and A. J. F. PRAXEDES, *Mol. Phys.* **52** (1984), 1125.
[4] J. W. GADZUK, *Comm. At. Mol. Phys.* **16** (1985), 219.
[5] C. BACKX, C. P. M. DE GROOT and P. BILJOEN, *Surf. Sci.* **104** (1981), 300;
C. T. CAMPBELL, *Surf. Sci.* **173** (1986), L641.

[6] PAN HAOCHANG, T. C. M. HORN and A. W. KLEYN, *Phys. Rev. Letters* **57** (1986), 3035.
[7] A. D. TENNER, K. T. GILLEN, T. C. M. HORN, J. LOS and A. W. KLEYN, *Phys. Rev. Letters* **52** (1984), 2183; *Surf. Sci.* **172** (1986), 90.
[8] C. BRUNNEE and H. VOSHAGE, *Massenspektrometrie* (Karl Thiemig, Muenchen, 1964).
[9] ROBERT G. WILSON and GEORGE R. BREWER, *Ion Beams With Application to Ion Implantation* (John Wiley and Sons, New York, 1973) Chap. 2.
[10] G. J. SCHULZ, *Rev. Mod. Phys.* **45** (1973), 423.
[11] A. VON ENGEL, *Ionized Gases* (Oxford University Press, London, 1965).
[12] D. W. O. HEDDLE, *J. Phys. E: Sci. Instr.* **4** (1971), 981.
[13] E. H. A. GRANNEMAN and M. J. VAN DER WIEL, in: *Handbook on Synchroton Radiation*, ed. E. E. Koch (North-Holland, Amsterdam, 1983), p. 367.
[14] W. HEILAND and E. TAGLAUER, in: *Methods of Experimental Physics*, vol. **22**, chap. 6.
[15] P. J. VAN DEN HOEK, T. C. M. HORN and A. W. KLEYN, to be published in *Surf. Sci.*
[16] C. T. CAMPBELL, *Surf. Sci.* **157** (1985), 43.